Available online at www.sciencedirect.com
ScienceDirect
International Journal of Mass Spectrometry 260 (2007) 121–127
International Journal of Mass Spectrometry
www.elsevier.com/locate/ijms

Lipid imaging in the zebra finch brain with secondary ion mass spectrometry

Kensey R. Amaya [a], Eric B. Monroe [b], Jonathan V. Sweedler [b], David F. Clayton [a,*]

[a] *Department of Cell and Developmental Biology, University of Illinois, Urbana-Champaign, 601 S. Goodwin Avenue, Urbana, IL 61801, United States*
[b] *Department of Chemistry, University of Illinois, Urbana-Champaign, 600 S. Matthews Avenue, Urbana, IL 61801, United States*

Received 7 July 2006; received in revised form 14 September 2006; accepted 22 September 2006
Available online 13 November 2006

Abstract

Lipids have diverse functions in the nervous system, but the study of their anatomical distributions in the intact brain is rather difficult using conventional methodologies. Here we demonstrate the application of high resolution time-of-flight (ToF) secondary ion mass spectrometry (SIMS) to image various lipid components and cholesterol across an entire brain section prepared from an adult zebra finch (*Taeniopygia guttata*), with a spatial resolution of 2.3 μm, resulting in the formation of 11.5 megapixel chemical images. The zebra finch is a songbird in which specific neural and developmental functions have been ascribed to discrete "song control nuclei" of the forebrain. We have observed a relative increase of palmitic acid C16:0 and oleic acid C18:1 in song control nuclei versus the surrounding tissue, while phosphate (PO_3^-), representative of phospholipids, was lower in these regions. Cholesterol was present at a high level only in the white matter of the optic tectum. More diffuse distributions were observed for stearic, arachidonic, linolenic, and palmitoleic acids. The presented results illustrate that SIMS imaging is a useful approach for assessing changes in lipid content during song circuit development and song learning.

Keywords: SIMS; Songbird; Brain; Lipid; Mass spectrometric imaging

1. Introduction

Lipids comprise a diverse array of molecular forms and are important in multiple aspects of brain development and brain function [1–7]. Many lipids have complex regional and subcellular distributions, but approaches for analyzing these distributions have been limited primarily to crude dissection and biochemical fractionation techniques [8], or fluorescent imaging techniques that require the chemical modification of native lipids [9–11], which may modify their biological properties [10–12].

In recent years, mass spectrometric imaging has emerged as a discovery tool to uncover the distribution of small molecules in biological tissues. Time-of-flight secondary ion mass spectrometry (ToF-SIMS) eliminates the need for any chemical labeling, tissue homogenization, or analyte preselection, and can provide both chemical specificity and the spatial distributions of endogenous compounds on the surface of a biological sample. A chemical image is created by scanning a mass spectrometric data-acquisition point in a raster pattern across the tissue and collecting a complete mass spectrum for each individual location. This enables the construction of tens to hundreds of chemically specific images of both known and uncharacterized compounds from a single experiment. ToF-SIMS can yield a spatial resolution of a micron or better, and has been applied to elemental imaging of single cells [13,14] as well as molecular imaging in drug delivery systems [15], kidney [16], nervous tissue [17] and single neurons [18], rat pheochromocytoma (PC12) cells [19], leukocytes [20], paramecia [21], *Tetrahymena* [22], and liposomes [23]. Recent developments of gold and cluster ion sources have increased the mass range available for analysis using ToF-SIMS to an upper limit of >1000 Da.

In this work, we apply ToF-SIMS imaging to the study of fatty acid distribution within the brain of the zebra finch (*Taeniopygia guttata*), a songbird. The zebra finch is an important model for neural circuit development, neurogenesis, and learning and memory (for comprehensive reviews see [24,25]). A male zebra finch learns to sing during a critical period in juvenile development. Song production is under the control of an interconnected

* Corresponding author. Tel.: +1 217 244 3668; fax: +1 217 244 5180.
E-mail address: dclayton@uiuc.edu (D.F. Clayton).

1387-3806/$ – see front matter © 2006 Elsevier B.V. All rights reserved.
doi:10.1016/j.ijms.2006.09.032

set of anatomically discrete, circumscribed nuclei in the telencephalon. These nuclei comprise the "song circuit" and are found only in songbirds. The output nucleus of the circuit, RA (robust nucleus of the arcopallium), receives a major axonal projection from another nucleus [26] known formally as HVC [27]. This projection is never completed in females of this species, who do not sing. Both RA and HVC are large and easy to visualize, even in unstained brain sections. Molecular genetic [28,29] and cell culture [30,31] analyses have suggested the potential involvement of various lipids and neurosteroids in the formation and function of the song circuit. Hence, the ability to identify and localize these small molecules within specific song nuclei would be of great benefit to further research.

Here we show the high resolution chemical imaging of a complete sagittal section of the songbird brain resulting in the creation of ion images, consisting of 11.5 megapixels each, for several fatty acids, as well as phosphate and cholesterol, at a spatial resolution of 2.3 μm. Ion images corresponding to palmitic acid (C16:0) and oleic acid (C18:1) show increased presence in the song nuclei HVC and RA while phosphate (PO_3^-) was decreased in comparison to the surrounding tissue. Several other lipids and cholesterol also show interesting localizations across the tissue section. By combining high resolution chemical imaging with a tiling procedure to produce very large ion images, both gross morphological features and small-scale distribution patterns are observed.

2. Experimental materials and methods

2.1. Brain collection and sectioning

Adult zebra finches, *Taeniopygia guttata* (>90 days of age), were sacrificed by decapitation and the brain removed. Brains were rapidly frozen on dry ice and stored at −80 °C until needed. A small drop of embedding media was used to affix the brain to the stage of a HM 550 ultramicrotome (Microm International, Walldorf, Germany) for sectioning. Tissues were not completely embedded in the media as this may have caused significant suppression of analyte signals acquired from the biological samples [32,33]. Sections (20 μm, parasagittal plane with the posterior and anterior areas of the section ∼1.5 mm and ∼1.7 mm from the midline) were collected at −14 °C using a 7° sectioning angle. Sections containing the song nuclei HVC and RA, from the brain hemisphere not in contact with the embedding material, were collected on glass slides and stored at −80 °C. Sections adjacent to those used for ToF-SIMS analysis were collected and verified to contain the HVC and RA song nuclei via cresyl violet staining (Fig. 1). All presented figures are from a single animal although similar distribution patterns were observed in sections from two other animals.

2.2. Histological staining

Sections were stained for cell nuclei and nucleoli with cresyl violet. Sections were first fixed in a solution of 4% paraformaldehyde dissolved in 100 mM phosphate buffer (final pH ∼7.2) for 5 min. Sections were then placed in 25 mM phosphate buffered saline for 2 min followed by 2 min in ddH_2O. Tissues were stained for 10 min in 0.1% cresyl violet and then dehydrated sequentially in 70%, 95%, and 100% ethanol and cleared for 5 min in Citrisolv (Fisher Scientific, Rochester, NY). Samples were then mounted with a cover slip using Permount.

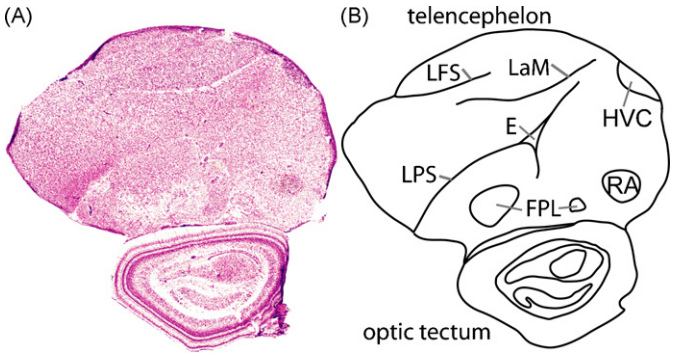

Fig. 1. Morphological features are identified via (A) the cresyl violet staining of a section adjacent to that used for ToF-SIMS analysis. (B) A schematic representation illustrating the complex morphology of the imaged tissue section that contains the robust nucleus of the archistriatum (RA), high vocal center (HVC), fasciculus prosencephali lateralis (FPL), entopallium (E), lamina pallio-subpallialis (LPS), lamina mesopallialis (LaM), and lamina frontalis superior (LFS).

2.3. ToF-SIMS analysis

Immediately prior to analysis, sections were removed from a −80 °C freezer and warmed under vacuum for 45 min and coated with a 1 nm deposition of Au using a Desk II TFC sputter coater (Denton Vacuum, Moorestown, NJ). ToF-SIMS analyses were performed with a TRIFT ToF-SIMS mass spectrometer (Physical Electronics, Chanhassen, MN) equipped with a gold liquid metal ion cluster source operating at 22 keV. The Au_2^+ primary ion beam was randomly rastered in a 256 × 256 pixel region at 8 kHz with an 8 ns pulse-width in unbunched mode. Total ion doses were kept well below the static limit of 1×10^{13} primary ions cm^{-2} ($\sim 3 \times 10^9$ cm^{-2}). Negative secondary ions (*m/z* 0.1–2000) were collected for 194 individual 600 μm × 600 μm tiles located across the sample in an ordered raster pattern with a 2–15% overlap between tiles without charge compensation. Mass spectra were internally calibrated using the Au^-, Au_2^-, and Au_3^- peaks. Images of these ions showed a homogenous distribution across the sample, suggesting that no artifacts were created as a result of sample coating.

2.4. Image analysis and stitching

Ion images, assembled using WinCadence software (Physical Electronics) for each individual tile, were created for the following compounds: phosphate PO_3^- (*m/z* 79.0), cholesterol (*m/z* 385.4), arachidonic acid C20:4 (*m/z* 303.2), palmitic acid C16:0 (*m/z* 255.2), palmitoleic acid C16:1 (*m/z* 253.2), stearic acid C18:0 (*m/z* 283.3), oleic acid C18:1 (*m/z* 281.2), linoleic acid C18:2 (*m/z* 279.23), and α-linolenic acid C18:3 (*m/z* 277.2). All images were created using the same relative intensity scale to enable the individual image tiles to be combined into an ion

image for the entire tissue section. Individual ion images for each compound were combined using VLmerge (an opensource software produced by the Imaging Technology Group at the Beckman Institute, University of Illinois at Urbana-Champaign) to produce an ion image consisting of ~11.5 megapixels for each compound. Slight fluctuations in ion yields were observed in several tiles due to fluctuations in primary ion current, although this effect did not inhibit analyses.

3. Results

3.1. Tissue staining and morphology

A tissue section adjacent to the one used for ToF-SIMS analysis was stained using cresyl violet to enhance the visualization of gross histological structure (Fig. 1). The song nuclei HVC and RA characteristically stain more darkly than surrounding tissue. Also visible are striations corresponding to the lamina pallio-subpallialis (LPS), lamina frontalis superior (LFS), and the lamina mesopallialis (LaM). The morphological complexity of the tissue section allows for the analysis of many different features with ToF-SIMS within a single experiment.

3.2. Chemical imaging

Chemical images were produced for several compounds across the tissue section as outlined below. Each image is the reconstruction of 194 individual 256 × 256 pixel images at a spatial resolution of 2.3 μm. A partial mass spectrum from a single 600 μm × 600 μm tile, which is the sum of 65,536 individual mass spectra, is presented in Fig. 2. Mass spectra from each tile produced hundreds of signals over the collected mass range. Many of these signals consisted of various fragment products formed during the desorption process while other components ionized intact and produced ion currents of adequate strength to allow for their imaging. Some ions had homogenous distributions across the tissue (not shown). Imaged ions were selected for detailed analysis based on their biological significance, strength of ion signal, and interesting distribution across the tissue section, and were identified on the basis of mass matches to previously reported fatty acid and cholesterol signals [17,34].

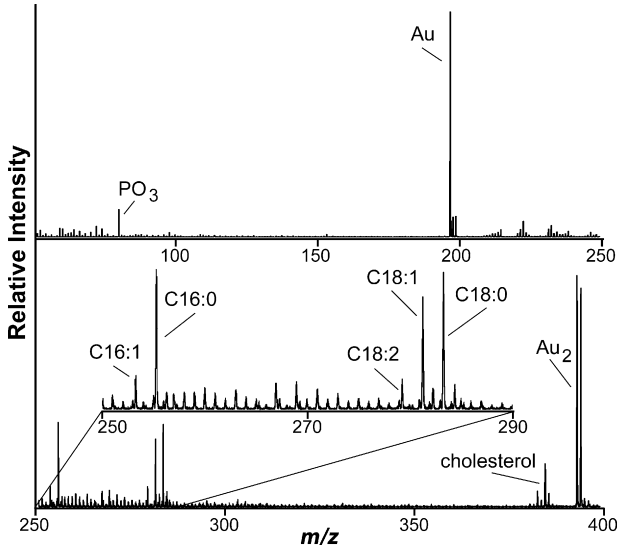

Fig. 2. Mass spectrum from a single 600 μm × 600 μm region of the songbird brain at the junction between the optic tectum and telencephalon illustrating many of the imaged lipid signals, as well as cholesterol, and both Au^- and Au_2^-.

3.2.1. Phosphate (PO_3^-)

The signal for phosphate (PO_3^-, *m/z* 79.0), which is believed to be indicative of membrane phospholipids, is strong throughout the tissue and presents distinctive morphological details (Fig. 3A). The song nuclei HVC and RA are marked by a decrease in intensity compared to the surrounding tissue (Figs. 3A and 4B). The LPS, fasciculus prosencephali lateralis (FPL), LFS, entopallium (E), and LaM also show a decrease in the phosphate distribution.

3.2.2. Cholesterol

Cholesterol (*m/z* 385.4) is found to be present at the highest levels in the optic tectum (Fig. 3B). More precisely, the distribution corresponds to regions of white matter comprised largely of myelinated axons. Increased cholesterol in the white matter has previously been observed in mouse brain, where it is believed to be associated with myelin [17]. In addition, cholesterol also appears to have an enhanced presence in another region enriched for fibers, the tract FPL [35].

3.2.3. Arachidonic acid

The polyunsaturated fatty acid, arachidonic acid (C20:4, *m/z* 303.2), generates a weak but granular signal, distributed evenly across this section with no strong anatomical localization (Fig. 3C). There is a slight increase in the caudal forebrain not observed with the other lipids (suggesting possible biological significance as opposed to experimental artifact) and a slight relative decrease in RA.

3.2.4. C16 lipids

Signal corresponding to the 16-carbon saturated fatty acid, palmitic acid (C16:0, *m/z* 255.2), is increased in the song nuclei HVC and RA compared to the surrounding tissue (Figs. 3D and 4C), suggesting that palmitic acid is enriched in these nuclei. Moreover, close inspection reveals a relative increase along the dorsal external edge of RA, an area apparently corresponding to the "cup" of RA which receives a developmentally and functionally distinct set of inputs from HVC [30,36,37]. Increased signal is also seen in E. The monounsaturated form, palmitoleic acid (C16:1, *m/z* 253.2), presents a similar distribution within the tissue section (Fig. 3E), although with a lower signal intensity. Several discrete points or lines of increased signal are observed around the rim of the section and are generally present in the other images. This artifact is due largely to an increased background signal along the edges of the tissue and from the substrate, as verified by observing the mass spectra from these regions.

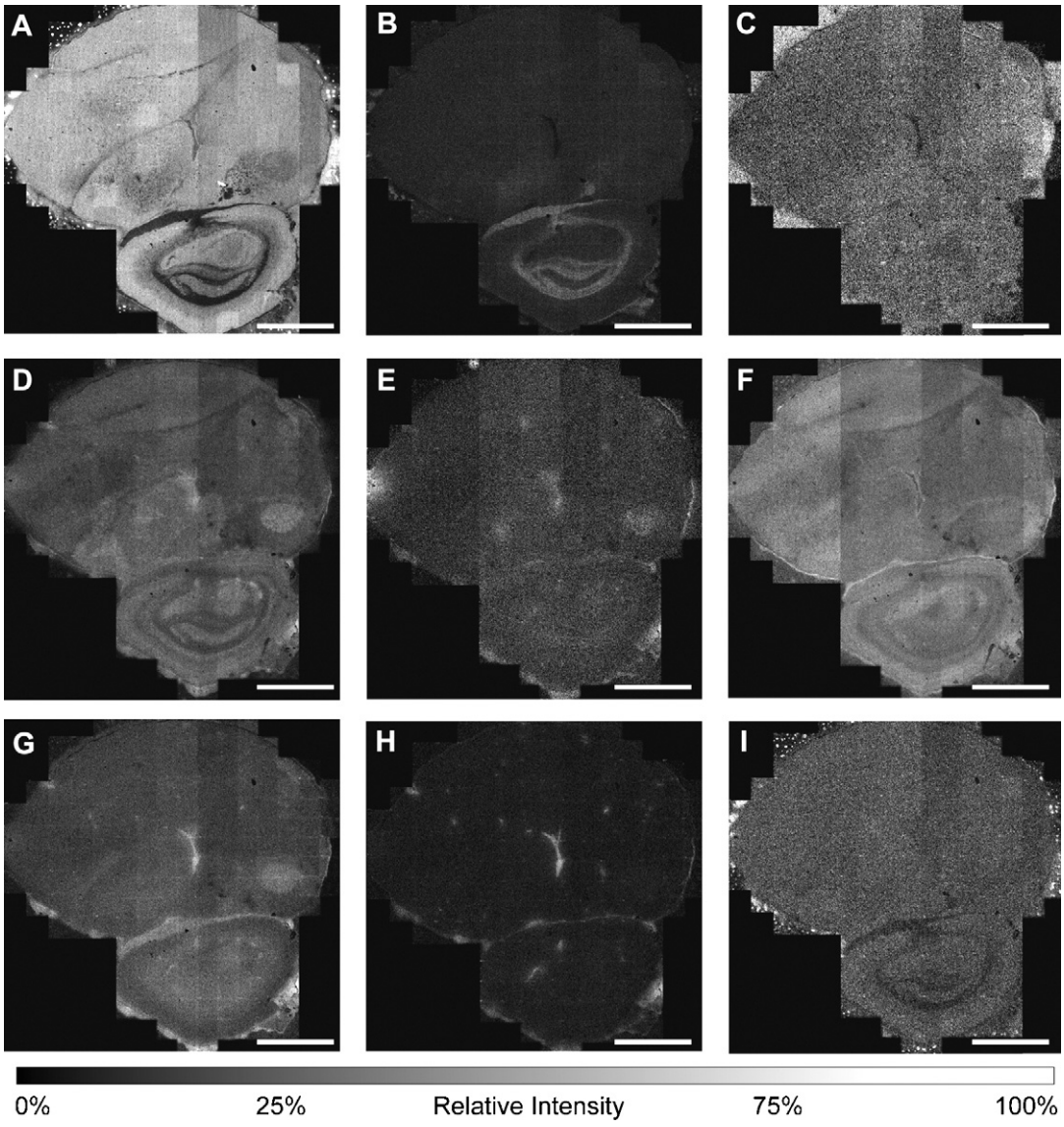

Fig. 3. Selected ion images from the songbird brain. Each ion image consists of ~11.5 million pixels within the tissue section and is the combination of 194 individual 600 μm × 600 μm ion images prepared on the same relative intensity scale. Ion images are (A) phosphate PO_3^- (*m/z* 79.0); (B) cholesterol (*m/z* 385.4); (C) arachidonic acid C20:4 (*m/z* 303.2); (D) palmitic acid C16:0 (*m/z* 255.2); (E) palmitoleic acid C16:1 (*m/z* 253.2); (F) stearic acid C18:0 (*m/z* 283.3); (G) oleic acid C18:1 (*m/z* 281.2); (H) linoleic acid C18:2 (*m/z* 279.23); and (I) α-linolenic acid C18:3 (*m/z* 277.2). Scale bars = 2 mm. (Full size ion images are available as supplemental materials online.).

3.2.5. C18 lipids

We analyzed signals for four, 18-carbon fatty acids of increasing unsaturation: stearic acid (C18:0, *m/z* 283.3), oleic acid (C18:1, *m/z* 281.2), linoleic acid (C18:2, *m/z* 279.2), and α-linolenic acid (C18:3, *m/z* 277.2). Interestingly, each of these compounds has a different distribution pattern. Stearic acid shows some enrichment in a region around the caudal edge of song nucleus RA, as well as in the dorsal telencephalon (superficial to LaM) (Fig. 3F). The monounsaturated fatty acid, oleic acid (C18:1), is present at a high level in regions identified as HVC, RA and E (Fig. 3G, see also Fig. 4D). The pattern is superficially similar to that for palmitic acid (Figs. 3D and 4C) but close inspection shows several differences—a complementary distribution within the center of E, no contrast along the lamina LaM and LFS, and less differentiation within the optic tectum. Linoleic acid (C18:2) localizes to several relatively small points of uncertain biological interpretation (Fig. 3H). Fig. 3I illustrates the distribution of the polyunsaturated lipid, α-linolenic acid (C18:3), and shows no strong localization in the brain section, although it is reduced in tectal layers that correspond to white matter.

4. Discussion

4.1. Lipid distribution patterns and biological significance

The ability to relate specific chemical composition to anatomically defined morphological features in complex tissues represents one of the largest benefits of high-resolution chemical imaging approaches. In this study, multiple chemical images

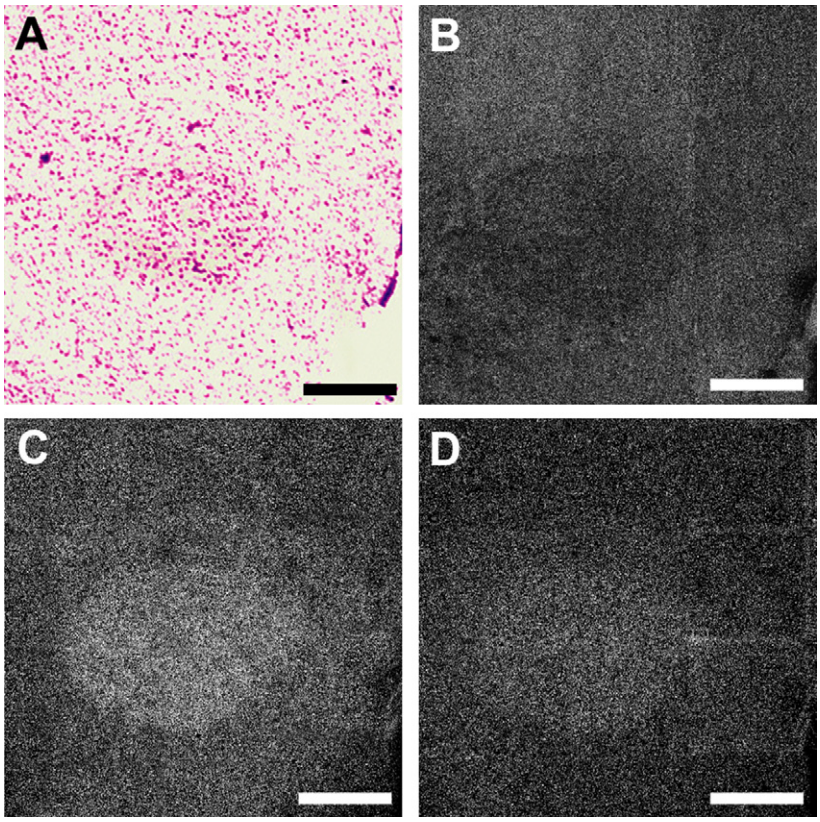

Fig. 4. Selected images of the region including the song nucleus RA. (A) Cresyl violet histological stain of section adjacent to the one in B–D; (B) phosphate (PO_3^-, *m/z* 79); (C) palmitic acid C16:0 (*m/z* 255); and (D) oleic acid C18:1 (*m/z* 281). Scale bars = 500 μm.

were produced from a single zebra finch brain section in its entirety, allowing the detection and comparison of the distribution of phosphate ion, cholesterol, and seven different lipids naturally present in the section. Analyses of similar sections from two other animals produced similar chemical images but are not shown here. The results reveal major differences in the distributions of these components.

Using the song nucleus RA as a focal point, some components are locally enriched, some locally impoverished, and others do not distinguish the nucleus from the surrounding tissue. RA is specifically enriched in three fatty acids—palmitate C16:0 (Fig. 4C), palmitoleate C16:1, and oleate C18:1 (Fig. 4D). Signals from phosphate (Fig. 4B) and arachidonic acid, however, are relatively decreased in RA. Palmitate is also relatively enriched in the "cup" structure along the dorsal edge, which may represent a projection terminus from HVC [30].

The polyunsaturated fatty acids, linoleic C18:2 and α-linolenic acid C18:3, all have relatively low signal intensity and little or no significant spatial localization. Linoleic acid does, however, localize in the area identified as E. Low signal intensity may be indicative of low concentration or low negative ionization of these lipids under the SIMS process. This is the first report of any specific lipid content in the song control system, although prior studies have indicated significant roles for lipid-binding proteins [28,29] and steroid-synthesis enzymes [30,31]. This technique may make possible the systematic analysis of how lipids themselves may change in the song system in significant ways during song learning and circuit development.

Cholesterol is of particular interest for songbird neurobiology as it is a steroid precursor, and localized production of steroids within the brain appears to be important for development of the song control pathway in males. Might ToF-SIMS be used to identify and map the distribution of neurosteroids? These compounds are likely present in much lower concentrations than cholesterol and may be below the detection level of ToF-SIMS. Continued improvements in the sensitivity of analyses and the observation of both positive and negative ions from a section may, however, help meet this challenge.

Except for cholesterol, all imaged analytes may be found in tissue as covalently linked moieties in larger compounds. At the subcellular level, these analytes are expected to be present in cellular membranes but are not necessarily limited to the cell membrane. Free fatty acids may occur as intermediary metabolites but are also components of phospholipids (major components of cell membranes) and triglycerides (energy stores). The degree to which the presented signals are from free analytes, or are fragmentation products as a result of the desorption process, is not currently known. Phosphate, for instance, serves as a marker of phospholipids, although other cellular sources (e.g., nucleic acids) may also contribute. Cholesterol is considered a ubiquitous component of cell membranes, yet it shows one of the most restricted distributions we observed, virtually the inverse of phosphate. Conclusively identifying the source of a signal is difficult and was not performed in these experiments as the imaging is meant to serve as a discovery tool to uncover any lipid heterogeneities and

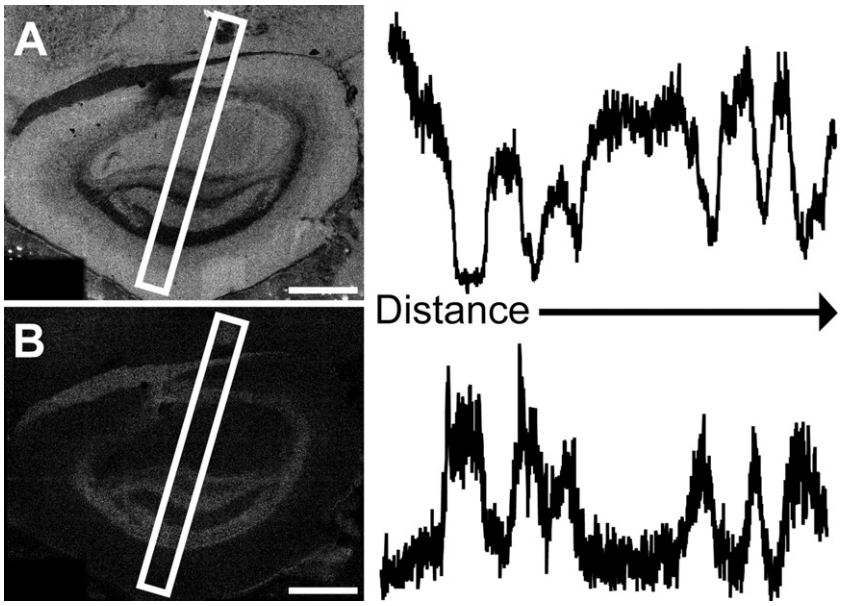

Fig. 5. Linescans of (A) phosphate PO_3^- (*m/z* 79.0) and (B) cholesterol (*m/z* 385.4) from the optic tectum illustrate the complementary distribution of these two compounds. Linescans begin in the lower portion of the midbrain and extend up and to the right as outlined in the ion images. Scale bars = 1 mm.

to guide further, more directed studies into the underlying biology.

The complementary distributions of phosphate and cholesterol within the optic tectum are highlighted by a linescan analysis of the image (Fig. 5). As the linescan crosses a region of the brain that contains white matter, the cholesterol signal rises while the phosphate signal decreases. The opposite is true for regions of grey matter that are rich in cell bodies. Previous studies have noted the enrichment of cholesterol in white matter and have attributed this to the concentrations of cholesterol in myelin [38]. Although linescans provide limited relative quantitative information, in this case from the optic tectum, further quantitation is hindered due to variability in ion yields across multiple tissue types and the low ion yields. Absolute quantitation for direct tissue samples is problematic for unlabeled compounds with MS in general, and in particular for SIMS, as many factors affect the ionization efficiency. However, relative quantitative comparisons of different regions may be performed by first normalizing ion images to a ubiquitous signal to remove any artifacts caused by sample preparation or topography [18,22]. Extended periods of ion collection would enable such relative comparisons but were not performed in this set of experiments.

4.2. Application of chemical imaging to tissue analysis

The chemical imaging of many compounds simultaneously and at high spatial resolution presents several challenges in regard to sample preparation, as well as other experimental considerations. In the experiments here, the tissue samples were flash-frozen immediately after dissection to minimize analyte redistribution. In addition, sample manipulations for the ToF-SIMS were kept to a minimum to prevent the loss and redistribution of analytes and to minimize the introduction of contaminants. With this conservative approach we appear to have achieved good reproducibility of results, as we observed similar distribution patterns for all studied compounds within the song nuclei RA and HVC of three separate birds.

Relatively abundant signals, such as those from the phosphate ion, produce images that can be magnified substantially to the point at which cellular-level detail begins to emerge (Fig. 6). In the reconstructed image of phosphate, the heterogeneous distribution is apparent across the tissue (Fig. 6A). When fewer and fewer tiles are included in the image (49 tiles in Fig. 6B and 9 in Fig. 6C), the broad features present in the FPL are more difficult to distinguish and identify. The small-scale fluctuations in phos-

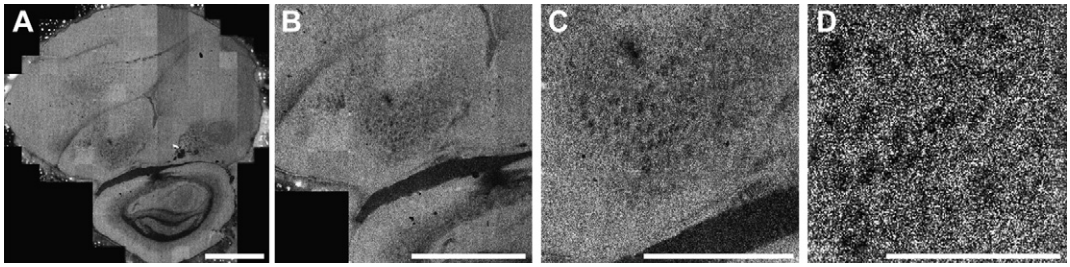

Fig. 6. Sequential zoom of the phosphate ion image (*m/z* 79.0) in (A) the full tissue image with all 194 tiles (scale bar = 2mm); (B) 49 central tiles (scale bar = 2mm); (C) 9 tiles (scale bar = 1 mm); and (D) a single tile (scale bar = 500 μm). The increasing levels of zoom reduce the overall image contrast from that observed in the larger images, but also allow the visualization of smaller features within the sample, including what appear to be the outline of individual cells.

phate signals are still observable in the single 600 μm × 600 μm image presented in Fig. 6D. Despite the low ion count and few pixels, the observed features appear to be single cells that have been sectioned within the tissue. This conclusion is based on the size and the characteristic phosphate signal that arises from the phospholipids in the cellular membrane. Although challenging, the high-resolution megapixel chemical imaging of entire tissue sections allows for not only the observation of gross chemical distributions and morphology but also fine details that would not be visible at lower resolutions.

For analytes present in only small quantities such as arachidonic acid, detection might be improved by using a larger beam-diameter or higher primary ion current to desorb more analyte molecules per mass spectrum – but at the expense of reduced spatial resolution – and by extending the period of data acquisition to more closely approach the static limit. Applications of higher mass cluster ion sources may also further improve the molecular imaging of intact lipids in the songbird brain.

5. Conclusions

The high-resolution chemical imaging of a complete sagittal section of the brain from the zebra finch, *Taeniopygia guttata*, reveals varied distributions of C16 and C18 saturated and mono-unsaturated fatty acids. The localizations of palmitic, palmitoleic, and oleic acids in the song nuclei are particularly interesting as these nuclei are intensively studied focal points for research into both neural development and adult plasticity. The results demonstrate the creation of chemical tissue maps that reach into the megapixel range with regard to the number of obtained mass spectra. Thus, the distribution of a large number of chemical components may be studied on both the gross morphological and micron level spatial scales within a single experiment.

Acknowledgments

We thank Charles Conway for assistance with the image stitching and Timothy Spila for technical assistance with the ToF-SIMS. This material is based upon work supported by the Initiative for Future Agriculture and Food Systems (grant no. 2001-52100-11527) from the USDA Cooperative State Research, Education and Extension service (D.F.C.), and the NIH through award nos. P30 DA018310 to the UIUC Neuroproteomics Center on Cell to Cell Signaling, and R01 DA017940 (J.V.S.). This work was carried out in the Center for Microanalysis of Materials, University of Illinois, which is partially supported by the US Department of Energy under grant DEFG02-91-ER45439. K.A. was supported by an Agricultural Genome Sciences and Public Policy Graduate Fellowship and by NIH R01 MH061994 (subcontract to D.F.C., PI: Barney Schlinger, UCLA).

Appendix A. Supplementary data

Supplementary data associated with this article can be found, in the online version, at doi:10.1016/j.ijms.2006.09.032.

References

[1] M.I. Aveldano, N.G. Bazan, Biochim. Biophys. Acta 296 (1973) 1.
[2] R.R. Baker, H. Chang, Can. J. Biochem. 58 (1980) 620.
[3] N.G. Bazan, Mol. Neurobiol. 32 (2005) 89.
[4] R.W. Gross, C.M. Jenkins, J. Yang, D.J. Mancuso, X. Han, Prostaglandins Other Lipid Mediat. 77 (2005) 52.
[5] H. Rosner, Prog. Mol. Subcell. Biol. 32 (2003) 49.
[6] P.S. Sastry, Prog. Lipid Res. 24 (1985) 69.
[7] T. Suzuki, Neurosci. Res. 44 (2002) 1.
[8] B.I. Roots, Neurochem. Res. 20 (1995) 1261.
[9] D. Huster, P. Muller, K. Arnold, A. Herrmann, Biophys. J. 80 (2001) 822.
[10] O. Maier, V. Oberle, D. Hoekstra, Chem. Phys. Lipids 116 (2002) 3.
[11] L. Kuerschner, C.S. Ejsing, K. Ekroos, A. Shevchenko, K.I. Anderson, C. Thiele, Nat. Methods 2 (2005) 39.
[12] R. Ishitsuka, A. Yamaji-Hasegawa, A. Makino, Y. Hirabayashi, T. Kobayashi, Biophys. J. 86 (2004) 296.
[13] J. Clerc, C. Fourre, P. Fragu, Cell Biol. Int. 21 (1997) 619.
[14] S. Chandra, D.R. Smith, G.H. Morrison, Anal. Chem. 72 (2000) 104A.
[15] A.M. Belu, M.C. Davies, J.M. Newton, N. Patel, Anal. Chem. 72 (2000) 5625.
[16] H. Nygren, P. Malmberg, C. Kriegeskotte, H.F. Arlinghaus, FEBS Lett. 566 (2004) 291.
[17] P. Sjovall, J. Lausmaa, B. Johansson, Anal. Chem. 76 (2004) 4271.
[18] E.B. Monroe, J.C. Jurchen, J. Lee, S.S. Rubakhin, J.V. Sweedler, J. Am. Chem. Soc. 127 (2005) 12152.
[19] T.P. Roddy, D.M. Cannon Jr., S.G. Ostrowski, N. Winograd, A.G. Ewing, Anal. Chem. 74 (2002) 4020.
[20] P. Sjovall, J. Lausmaa, H. Nygren, L. Carlsson, P. Malmberg, Anal. Chem. 75 (2003) 3429.
[21] T.L. Colliver, C.L. Brummel, M.L. Pacholski, F.D. Swanek, A.G. Ewing, N. Winograd, Anal. Chem. 69 (1997) 2225.
[22] S.G. Ostrowski, C.T. Van Bell, N. Winograd, A.G. Ewing, Science 305 (2004) 71.
[23] D.M. Cannon, M.L. Pacholski, N. Winograd, A.G. Ewing, J. Am. Chem. Soc. 122 (2000) 603.
[24] H.P. Zeigler, P. Marler, Ann. NY Acad. Sci. 1016 (2004) 1, xiii-xvii.
[25] E.A. Brenowitz, D. Margoliash, K.W. Nordeen, J. Neurobiol. 33 (1997) 495.
[26] F. Nottebohm, T.M. Stokes, C.M. Leonard, J. Comp. Neurol. 165 (1976) 457.
[27] A. Reiner, D.J. Perkel, L.L. Bruce, A.B. Butler, A. Csillag, W. Kuenzel, L. Medina, G. Paxinos, T. Shimizu, G. Striedter, M. Wild, G.F. Ball, S. Durand, O. Gunturkun, D.W. Lee, C.V. Mello, A. Powers, S.A. White, G. Hough, L. Kubikova, T.V. Smulders, K. Wada, J. Dugas-Ford, S. Husband, K. Yamamoto, J. Yu, C. Siang, E.D. Jarvis, J. Comp. Neurol. 473 (2004) 377.
[28] N.I. Denisenko-Nehrbass, E. Jarvis, C. Scharff, F. Nottebohm, C.V. Mello, Neuron 27 (2000) 359.
[29] J.M. George, H. Jin, W.S. Woods, D.F. Clayton, Neuron 15 (1995) 361.
[30] C.C. Holloway, D.F. Clayton, Nat. Neurosci. 4 (2001) 170.
[31] B.A. Schlinger, K.K. Soma, S.E. London, Trends Neurosci. 24 (2001) 429.
[32] R. Kruse, J.V. Sweedler, J. Am. Soc. Mass Spectrom. 14 (2003) 752.
[33] S.A. Schwartz, M.L. Reyzer, R.M. Caprioli, J. Mass Spectrom. 38 (2003) 699.
[34] D. Touboul, A. Brunelle, F. Halgand, S. De La Porte, O. Laprevote, J. Lipid Res. 46 (2005) 1388.
[35] A.D. Szekely, J.R. Krebs, J. Comp. Neurol. 368 (1996) 198.
[36] R. Mooney, M. Rao, J. Neurosci. 14 (1994) 6532.
[37] M. Konishi, E. Akutagawa, Nature 315 (1985) 145.
[38] G. Saher, B. Brugger, C. Lappe-Siefke, W. Mobius, R. Tozawa, M.C. Wehr, F. Wieland, S. Ishibashi, K.A. Nave, Nat. Neurosci. 8 (2005) 468.